Towards sibilant /s/ modelling: preliminary computational results

Xavier Grandchamp[a], Annemie Van Hirtum[a], Xavier Pelorson[a], Kazunori Nozaki[b] and Shinji Shimojo[b]

[a]Département Parole & Cognition, GIPSA-lab, 46, avenue Félix Viallet, 38031 Grenoble Cedex, France
[b]Cyber Media Center, Osaka University Cybermedia, 5-1 Mihogaoka Ibaraki, 567-0047 Osaka, Japan
xavier.grandchamp@gipsa-lab.inpg.fr

The importance of turbulence in human speech sounds production is generally accepted in the case of fricatives. Nevertheless, this phenomenon is margely taken into account in physical modelling of speech production. The current study considers steady flow at a given Reynolds number Re = 4000. Large Eddy Simulation has been used to simulate the flow evolution in case of two dimensional geometries. The used geometrical and flow characteristics are severe simplifications of the human upper airways beyond the glottis. The impact of those typical geometries on the computed flow field is searched in order to detect the aeroacoustical sources produced by turbulent flow, crucial in /s/ production. The presence of the obstacle in a uniform channel and the curved pipe induce reversed flow. Nevertheless, the turbulence intensity, in case of the obstacle configuration does not correspond with turbulent flow, whereas the curve tends to give higher turbulent velocities along the curvature.

1 Introduction

Human speech sounds can be classified into two distinctive categories depending on their production mode: voiced and unvoiced sounds. The production of voiced sound was deeply studied, and among of research is available in the literature. The airflow expulsed by the lungs interacts with the vocal folds leading to an auto-oscillation of the vocal folds. The other mechanism is purely aeroacoustics and corresponds to the production of unvoiced sound. Nevertheless, less attention was given to the mechanism of production of unvoiced sound. The complex geometry of the human upper airways, and the flow conditions yield the turbulent air flow. The importance of the turbulence in the production of unvoiced sound is noted [2]. Numerous experimental studies reveal the importance of the interaction between the flow and obstacle, in a.o [10, 12]. The mechanism of sound production and the importance of vorticity and the necessary flow-separation conditions in the production of fricatives are studied [7, 11]. The study of jet vorticity and its evolution for unvoiced sound production is summarised in [6] as "the sound field was seen to be determined uniquely by the interaction of jet vorticity and the shape of the vocal tract".

One of the main articulator concerning obstacle-flow interaction is the teeth. The impact of teeth on the production of sibilant /s/ is studied by [5, 9]. Large Eddy Simulation (LES) is applied on the mid-sagittal plane of a human oral cavity [9]. Nevertheless, the complexity of the geometry gave us a difficult understanding of the phenomena.

As a first step for a future application in speech production, the aim of this paper is to analyse with LES, the evolution of 2 dimensional laminar inflow in the case of schematic human upper airways. The influence of the vocal folds and false vocal folds are left untreated. The study is restricted on typical geometries present in the upper airways. A rectangular straight pipe, a rectangular straight pipe with an obstacle, and finally a rectangular curved pipe are considered. The three geometries are studied separately and their impact on the flow evolution is discussed.

The paper is organised as follows. Section 2 presents the numerical method and numerical domains. The results for the different geometries are discussed in section 3. The conclusion is formulated in section 4.

2 Computational Method

The airflow is simulated within the different geometries by using a commercial explicit finite element code "Front Flow Blue/ FFB", developed by Advance Soft Corporation [3]. In the following section the method is outlined [6]. Next, the computational domains are briefly presented.

2.1 Governing equations

This code solves spatially-filtered incompressible continuity equation and Navier-Stokes equations.

$$\frac{\partial \overline{u_i}}{\partial y_i} = 0, \tag{1}$$

$$\frac{\partial \overline{u_i}}{\partial t} + \frac{\partial}{\partial y_j}(\overline{u_i u_j} + \tau_{ij}) = -\frac{1}{\rho_0}\frac{\partial \overline{p}}{\partial y_j} + \frac{\partial}{\partial y_j}\left\{\nu(\frac{\partial \overline{u_i}}{\partial y_j} + \frac{\partial \overline{u_j}}{\partial y_i})\right\}, \tag{2}$$

p represents the grid-scale static pressure, ν the kinematic viscosity, u_i (i=1, 2, 3) corresponds to the grid scale velocity component. The subgrid-scale (SGS) stress tensor is defined by:

$$\tau_{ij} = \overline{u_i u_j} - \overline{u_i}\,\overline{u_j}. \tag{3}$$

The Smagorinsky closure is applied to the SGS stress τ_{ij}:

$$\tau_{ij} - \frac{1}{3}\delta_{ij}\tau_{kk} = -2\nu_{SGS}\overline{S}_{ij}, \tag{4}$$

Where

$$\nu_{SGS} = (C_s\Delta)^2|\overline{S}|, \ |\overline{S}| = \sqrt{2\overline{S}_{ij}\overline{S}_{ij}}, \ \overline{S}_{ij} = \frac{1}{2}(\frac{\partial \overline{u_i}}{\partial y_j} + \frac{\partial \overline{u_j}}{\partial y_i}) \tag{5}$$

C_s is the Smagorinsky coefficient and Δ is the size of the grid filter. In our case, the dynamic Smagorinsky model with modification due to [8] is used. C_s is determined locally in time and space by

$$C_s^2 = \frac{\langle M_{ij}l_{ij}\rangle}{2\Delta^2\langle M_{ij}M_{ij}\rangle}, \tag{6}$$

$$M_{ij} = \widetilde{\beta}_{ij} - \alpha^2 \left|\widetilde{\widetilde{S}}\right|\widetilde{\widetilde{S}}_{ij}, \quad \alpha \cong \frac{\widetilde{\widetilde{\Delta}}}{\widetilde{\Delta}} = 2, \qquad (7)$$

$$l_{ij} = (\widetilde{\gamma}_{ij} - \widetilde{\overline{u}}_i \widetilde{\overline{u}}_j) - \frac{1}{3}\delta_{ij}(\widetilde{\gamma}_{kk} - \widetilde{\overline{u}}_k \widetilde{\overline{u}}_k), \qquad (8)$$

Where $\beta_{ij} = \left|\overline{S}\right|\overline{S}_{ij}$ and $\gamma_{ij} = \overline{u}_i \overline{u}_j$. The symbol "~" represents a test-filtering operation, " $\langle \ \rangle$ " represents an averaging operation, and $\widetilde{\widetilde{\Delta}}$ is the size of the test filtered width. A fully implicit Crank-Nicolson scheme (CN) and explicit time streamline upwind scheme were employed for integrating the momentum equation. The spatial discretization is based on the Finite Element Method (FEM). The schemes have a second order accuracy in time and space.

2.2 Numerical domain and inflow

The three geometries taken into account in our study were created by using a commercial mesh generator developed by [4].

The following parameters were chosen constant for the different geometries: the dimensional height H of the rectangular pipe is equal to 0.025 m, the aspect ratio l/H, where l represents the width of the rectangular pipe is equal to l/H = 4. The uniform dimensional inlet velocity is constant and equal to $U_0 = 2.5$ m.s^{-1}. Therefore, the Reynolds number based on the inlet velocity and the height H is equal to Re = 4000. The nondimensional time increment corresponds to $\Delta t = 10^{-3} = \dfrac{U_0}{H} \cdot \Delta t$.

In the case of a rectangular straight pipe, the computational domain is [-2H, 2H] * [0, H] * [0, 5H] respectively in y_1, y_2 and y_3 direction, where y_1, y_2, y_3 represent respectively the lateral, the spanwise, and the streamwise coordinates. Structured meshes are used. The origin is located on the inlet face, at the centre of the lateral plan and the bottom side of the rectangular pipe, as shown in Fig. 2 (a). 74 elements are used in the streamwise direction and are uniformly distributed. 74 elements are used in the spanwise direction towards a symmetric tangent hyperbolic distribution. Δy_2, which represents the size of the first element near the wall is equal to $\Delta y_2 = 0.005H$. 50 elements are used in the spanwise direction. The total number of computational elements is approximately 280 000. The inlet velocity is imposed to be uniform. Non-slip condition was used on the wall. Non reflective conditions are used as exit conditions.

For the following case, an obstacle representing a schematic tooth is imposed. The dimensions of the computational domain in which the tooth is inserted is [-2H, 2H] * [0, H] * [0, 4.05H]. The tooth is located at a distance equal to $y_1 = 16/5H$. The geometry of the tooth is a trapezoid for which the base is 1.25/5H and its opposite side has a length of 0.25/5H; the upstream and downstream sides of the tooth make respectively an angle of 105° and 90° with the bottom wall. Its height is equal to 7/10H. Approximately 1 880 000 elements were used to compute the flow evolution. Structured meshes are still used. The computational domain is divided into 5 blocks as seen in Fig. 2 (b). Close to the

obstacle the grid meshes are refined in order to be small enough to resolve the boundary layer and bound vortices around the obstacle. The origin is located at the same position as for the previous case. The same inlet and boundaries conditions imposed for case1 are used.

The third geometry is a rectangular curved straight pipes linked with a curved pipe. The horizontal straight pipe has a computational domain [0, 2.5H] * [0.2H, 1.2H] *[0, 4H] respectively in y_1, y_2 and y_3 direction. The vertical straight pipe has a computational domain [-1.2H, -2H] * [0H, -2.5H] * [0H, 4H] in y_1, y_2 and y_3 direction. The origin is located on a bottom side of the horizontal rectangular straight pipe. The rectangular curved pipe is a quarter ring with an inner radius of 0.2H and an extern radius of 1.2H linking the pipes. 249 elements are used along the streamwise direction, 74 elements along the spanwise direction and 100 along the lateral direction. In this case, the origin is located at the bottom side of the horizontal rectangular straight pipe. The total number of computational elements is approximately 750 000. As for previous cases, the same inlet and boundaries conditions are used.
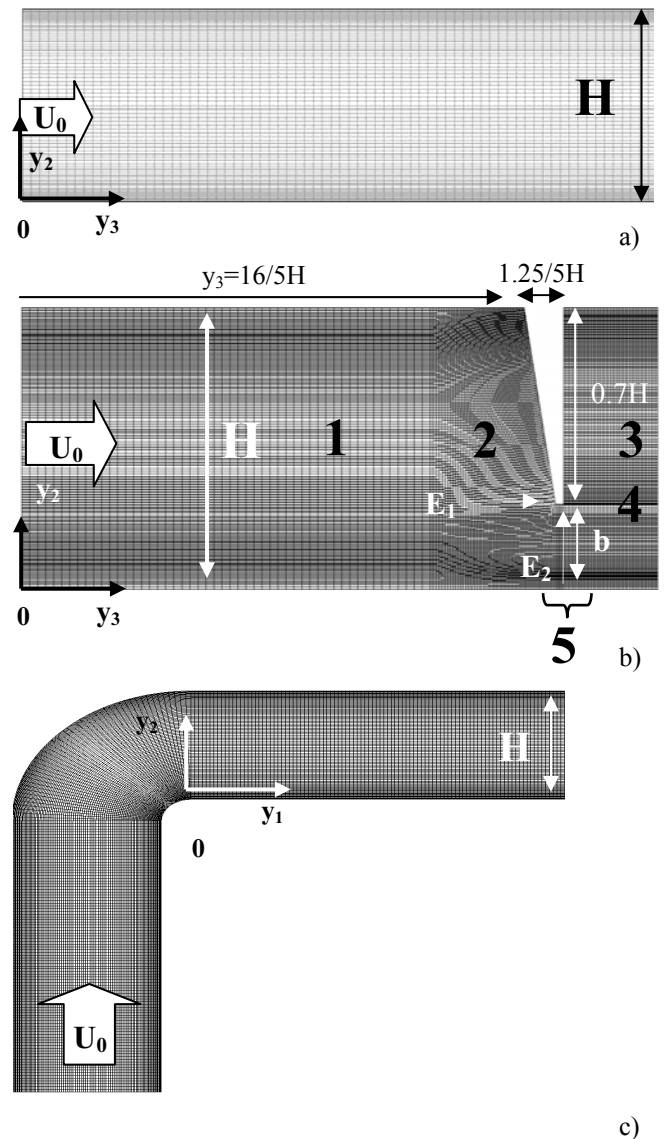
Fig. 2 Typical pipe geometries, a) rectangular straight b) rectangular straight + obstacle, c) rectangular curved.

3 Results and discussion

3.1 Rectangular straight pipe

The first results concern the basic representation of a rectangular straight pipe. This representation is viewed as the simplest simplification of the vocal tract. No perturbation due to upstream obstacle is assessed; therefore the flow is laminar. The main interest of such geometry resides in the certification of the code under use and as a reference case.

a)

b)
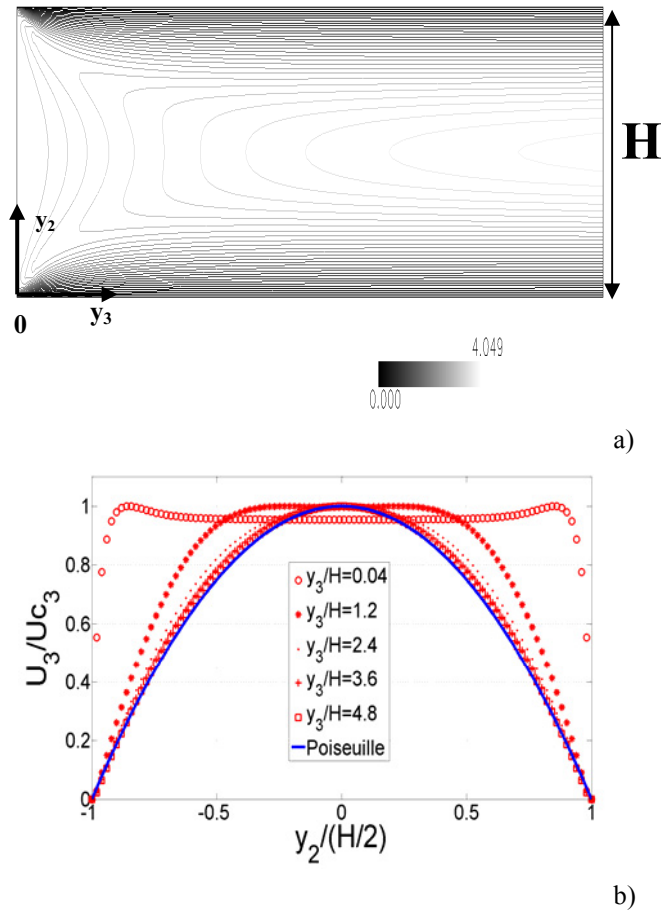
Fig. 3 Mean velocity evolution along the spanwise direction for different streamwise localisation. a) streamlines dimensional velocites U_3, b) mean velocity normalised with centreline velocity Uc_3.

Fig. 3(a) and 3 (b) represent the mean velocity along the spanwise direction. Fig. 3(b) shows the evolution of the streamwise component of the velocity normalised by its centreline velocity Uc_3. As the downstream localisation increases, the rectangular velocity profile imposed at the inlet tends to be transformed into the parabolic Poiseuille profile. In order to compare with the Poiseuille profile the origin of the axis where shifted to the centre of the rectangular pipe.

$$U_3 = \frac{3}{2} U_0 (1 - \frac{y_2^2}{\left(\frac{H}{2}\right)^2})$$ (9)

This evolution confirms boundary layer grows on both wall, due to viscosity, and mass-conservation.
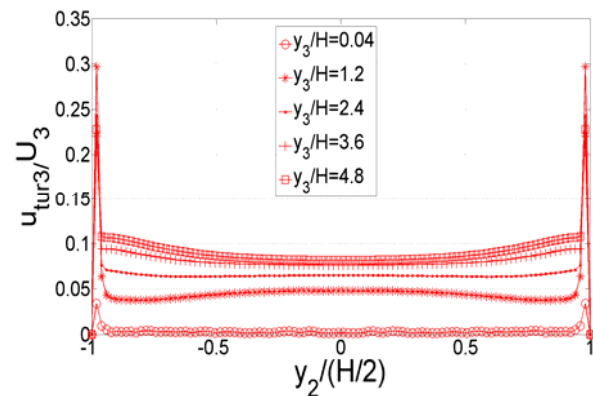
Fig. 4 turbulent intensity u_{tur3}/U_3 for different streamwise localisation.

As a further analysis, Fig. 4 presents the turbulence intensity u_{tur3}/U_3, where u_{tur3} represents the rms value of the streamwise component of the velocity along the rectangular straight pipe. The turbulence level is increased with the downstream localisation. The maximum values are observed close to the wall and comprised between $5\% < u_{tur\,3}/U_3 < 30\%$.

3.2 Rectangular straight pipe with an obstacle

This subsection presents the impact of an obstacle on the laminar inflow. Fig. 5 shows as the downstream location increases the flow becomes asymmetric. From $y_3/H = 1.8$, the position of the velocity maximum U is shifted to the flat wall. From Fig. 5 the flow maximum of the velocity is localised in an area which starts downstream the end of the obstacle and is equal to about 4 times the inlet velocity.

.
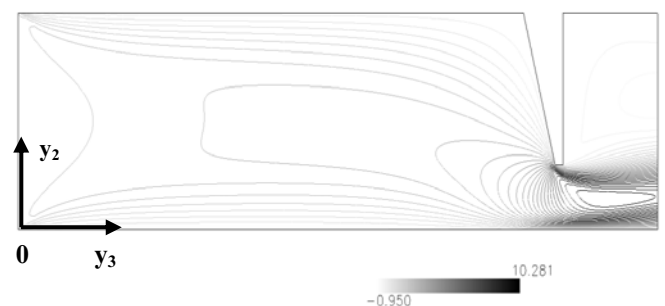
Fig. 5 Contourlines of the dimensional mean velocity U [m.s^{-1}].

Fig. 6, for which the axis are similar to Fig. 3, shows the flow evolution along the obstacle and reveals the existence of a recirculation zone, by the presence of negative velocities. The velocities in the recirculation zone are comprised between -0.75 m.s^{-1} < U < 0 m.s^{-1}.
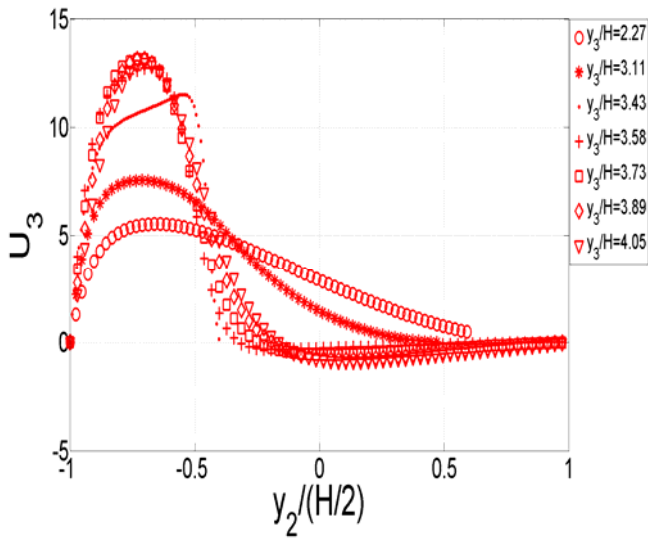
Fig. 6 dimensional mean velocities for different streamwise localization.

Fig. 7 presents the mean velocities profiles along the obstacle at different distance ΔE_1, where ΔE_1 represents the distance between the location of the velocity measurements and the edge E1. The flow is asymmetric, compared with the velocity profile before and after the obstacle, the maximum velocity is close to the obstacle and accelerated along the singularity.
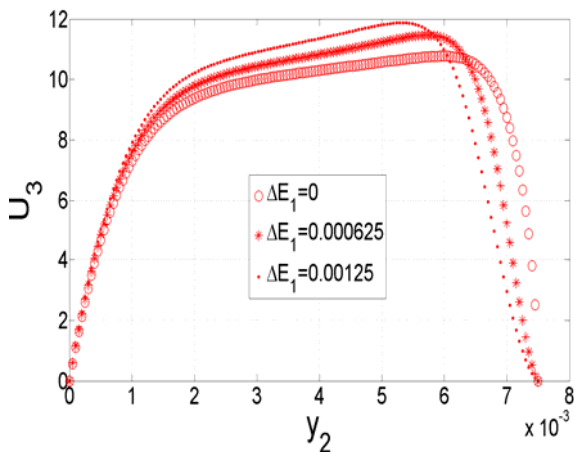
Fig. 7 velocity profiles at different distance ΔE_1.

Fig. 8 presents the turbulent intensity profiles along the obstacle. Except for $\Delta E_1 = 6.25*10^{-4}$ m, and at a distance equal to $5*10^{-3}$ m from the obstacle, the level of the turbulence intensity is very low, $u_{tur3}/U_3 < 1\%$. For this Reynolds number, and the configurations of the obstacle (shape and aperture) turbulent regime is not reached. The turbulence velocity u_{tur3} is seen to be $u_{tur3} \leq 0.218$ m.s^{-1} along the computational domain at ΔE_1.

Fig. 9 represents the mean velocity profiles at different downstream spanwise distances $\Delta E_2/b$, where ΔE_2 represents the distance between the location of the velocity measurements and the edge E_2, and b the distance between the obstacle and the opposite flat wall. We use as outer scaling, U_{3max} and $y_{2(1/2)}$, where U_{max} represents the maximum velocity of the streamwise component and $y_{2(1/2)}$ the distance between the two spanwise locations

corresponding to 50% of U_{3max}. The results are compared with data from an experimental study on turbulent wall jets,
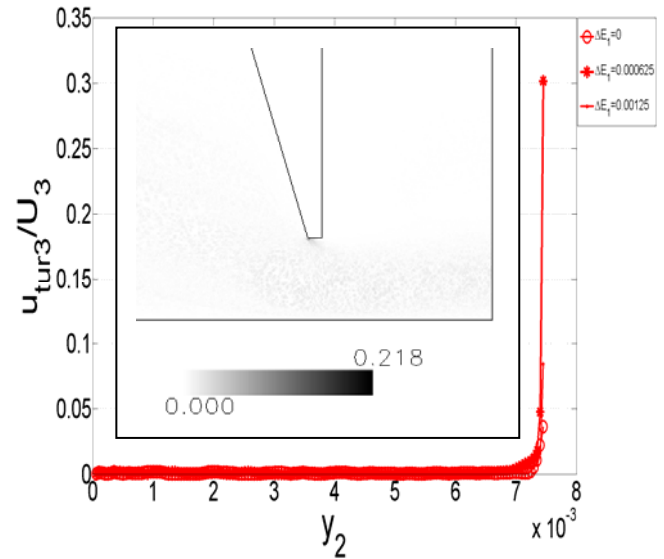
Fig. 8 Turbulent intensity profiles at different location ΔE_1.

for which Re = 9600 and b= $9.6*10^{-3}$ m [1]. Although, the profiles are close to the obstacle, it seems the flow tends to present a self-similar evolution comparable to a wall jet.
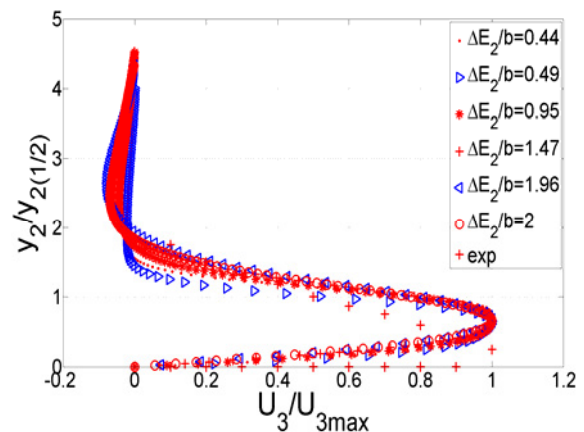
Fig. 9 Mean velocity profile at different downstream location $\Delta E_2/b$ l from the edge (E_2).

3.3 Rectangular curved pipe

The study of a curve, is motivated by the geometry of the vocal tract. In this section, we briefly give a qualitative presentation of the flow behaviour imposed by the curvature. From Fig. 10 a) the curve implies an increase of the velocity from the beginning of the curvature and a stall of the boundary layer leading to a recirculation zone which is zoomed on in Fig. 10 b). In Fig 11 it appears the curvature generates turbulent velocities area which propagates downstream the geometry. The magnitude turbulent velocities are comprised between 0 m.s^{-1} < u_{tur} < 1.861 m.s^{-1} which represent about 20% of the Mean velocity.

a)

b)
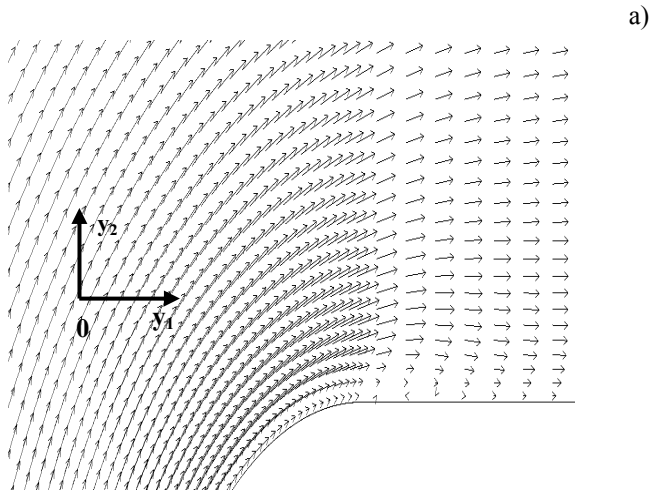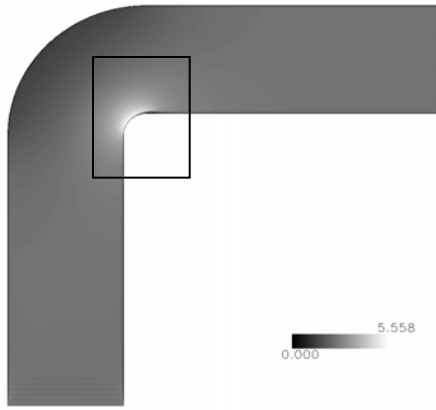
Fig. 10 a) Magnitude of the mean velocity b) Vectorial representation of the mean flow.
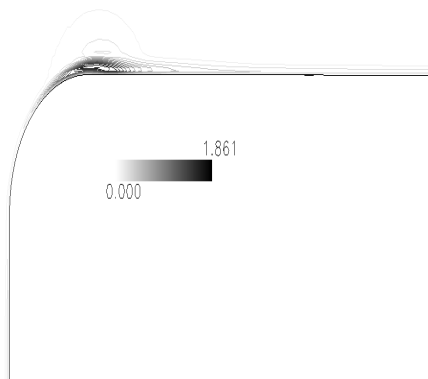
Fig. 11 Contours of the magnitude turbulent velocities.

4   Conclusion

The effects of typical articulator geometries, comparable to a tooth and a curve, on the flow field development of a 2 dimensional incompressible fluid flow were computed. For assessed flow characteristic and geometrical configurations, the obstacle generates lower turbulence than the curvature. Nevertheless, both geometries create an asymmetric flow

and lead to the creation of a recirculation zone. Therefore, further investigations are needed concerning the degree of constriction, the shape of the obstacle, the distance between the obstacle and the outlet.

Acknowledgments

References

[1] J.G. Eriksson, R. I. Karlsson, and J. Person, "An experimental study of a two-dimensional plane turbulent wall jet", *Exp. Fluids* 20, 50-60 (1998)

[2] G. Fant, Acoustic Theory of Speech Production (Mouton, the Hague) (1960)

[3] *FrontFlow/Blue version.4.0 User Manual*. Collaborative Research Center for Computational science and Technology, Institute of Industrial Science, the Universtiy of Tokyo, JAPAN. software@rss21.iis.u-tokyo.ac.jp

[4] *Gridgen Tutorial workbook.* version 15 volume3 gridgen@pointwise.com

[5] M. S. Howe, R. S. Gowan, " Aeroacoustics of /s/"*Pro. R. Soc. A.* 461,1005-1028 (2005)

[6] C. Kato, M. Kaiho, and A. Manabe, "An overset finite-element large-eddy simulation method with applications to turbomachinery and aeroacoustics", *J. Appl. Mech.* 70, 32–43 (2003)

[7] M. H. Krane, "Aeroacoustic production of low-frequency unvoiced speech sounds", *J. Acoust. Soc. Am.* 118, 410-427 (2005)

[8] D. K. Lilly, "A proposed modification of the Germano subgrid-scale closure method", *Phys. Fluids A* 4, 633-635 (1992)

[9] K. Nozaki H. Tamagawa and S. Shimojo, " Prediction of dental fricative sound by Lighthill ,– Curl equation", In *Proc. in. silico dentistry,* page 4, Osaka, Japan (2008)

[10] C. H. Shadle, "The Acoustics of Fricative Consonants", Ph.D. thesis, Massachusetts Institute of Technology (1985)

[11] D. J. Sinder, ''Synthesis of unvoiced speech sounds using an aeroacoustic source model'' , Ph.D. thesis, Rutgers University (1999)

[12] K. N. Stevens, ''Airflow and turbulence noise for fricative and stop consonants: Static considerations'', *J. Acoust. Soc. Am. 50,* 1180- 1192 (1971)